Wang *et al. Chin. J. Mech. Eng.* (2021) 34:101
https://doi.org/10.1186/s10033-021-00623-x

Chinese Journal of Mechanical Engineering

ORIGINAL ARTICLE

Open Access

Novel Traveling Wave Sandwich Piezoelectric Transducer with Single Phase Drive: Theoretical Modeling, Experimental Validation, and Application Investigation

Liang Wang[1,2*], Fushi Bai[2,3], Viktor Hofmann[3], Jiamei Jin[1] and Jens Twiefel[2]

Abstract

Most of traditional traveling wave piezoelectric transducers are driven by two phase different excitation signals, leading to a complex control system and seriously limiting their applications in industry. To overcome these issues, a novel traveling wave sandwich piezoelectric transducer with a single-phase drive is proposed in this study. Traveling waves are produced in two driving rings of the transducer while the longitudinal vibration is excited in its sandwich composite beam, due to the coupling property of the combined structure. This results in the production of elliptical motions in the two driving rings to achieve the drive function. An analytical model is firstly developed using the transfer matrix method to analyze the dynamic behavior of the proposed transducer. Its vibration characteristics are measured and compared with computational results to validate the effectiveness of the proposed analytical model. Besides, the driving concept of the transducer is investigated by computing the motion trajectory of surface points of the driving ring and the quality of traveling wave of the driving ring. Additionally, application example investigations on the driving effect of the proposed transducer are carried out by constructing and assembling a tracked mobile system. Experimental results indicated that 1) the assembled tracked mobile system moved in the driving frequency of 19410 Hz corresponding to its maximum mean velocity through frequency sensitivity experiments; 2) motion characteristic and traction performance measurements of the system prototype presented its maximum mean velocity with 59 mm/s and its maximum stalling traction force with 1.65 N, at the excitation voltage of 500 V_{RMS}. These experimental results demonstrate the feasibility of the proposed traveling wave sandwich piezoelectric transducer.

Keywords: Traveling wave, Sandwich piezoelectric transducer, Single phase excitation, Transfer matrix method, Ultrasonic motor

1 Introduction

Piezoelectric ceramic material utilizes its positive/converse piezoelectric effect to achieve the energy conversion between electric energy and mechanical energy, being one of commonly used smart materials in industry and research [1]. Piezoelectric transducer is the typical application of piezoelectric ceramic materials and can be employed as sensors or actuators, being widely applied to aerospace, optics, robotics, and biomedical engineering [2]. Some piezoelectric transducers utilizing the converse piezoelectric effect can convert electrical energy to micro-amplitude mechanical vibration energy, thereby they can be designed as the stator of ultrasonic motors [3]. Vibration characteristics of the piezoelectric transducers directly influence the mechanical output performance of ultrasonic motors. This is because the

*Correspondence: lwang@nuaa.edu.cn
[1] State Key Laboratory of Mechanics and Control of Mechanical Structures, Nanjing University of Aeronautics and Astronautics, Nanjing 210016, China
Full list of author information is available at the end of the article

micro-amplitude vibration of the piezoelectric transducer is transmitted to the macro motion of slider/rotor of ultrasonic motors by friction. Elliptical motion is one of the significant evaluation indexes for the vibration characteristics of the piezoelectric transducers. Therefore, how to construct efficient elliptical motion in the driving tip of the piezoelectric transducer is the key step of ultrasonic motor design.

In general, to generate the effective elliptical motion of the driving tip, the piezoelectric transducers are expected to operate in the coupling vibration mode [4]. This is because the elliptical motion of the driving tip is used to produce the friction between the stator and the rotor/slider of ultrasonic motors for achieving macro rotary/linear motion. Thus, the generation of the elliptical motion is significant for piezoelectric transducers. However, for producing the elliptical motion, two vibration modes are generally required to be stimulated and coupled in the piezoelectric transducers, increasing the difficulties of design, manufacturing, and assembling of transducer [5, 6]. Additionally, how to achieve the resonant frequency consistency of the two selected vibration modes is also a difficult issue for the control system of the piezoelectric transducers. To avoid these problems, single-phase excited piezoelectric transducer is the preferred option [7]. This is because this type of piezoelectric transducer only needs a phase drive signal to achieve the elliptical motion of its driving tip, eliminating the problem of adjusting resonant frequencies and simplifying the control system [8].

Researchers have made some efforts in the research of single-phase excited piezoelectric transducers [9–19]. Kurosawa et al. [9] used a small mass to attach in a ring type piezoelectric transducer, realizing two orthogonal vibration modes with a slightly different resonant frequency excited in the ring transducer under a single power supply. Therefore, a circular ultrasonic motor was constructed. Utilization of the structural property of rectangular piezoelectric plate and the asymmetrical resonant excitation, Vyshnevskyy et al. [10] proposed a single-mode linear ultrasonic motor. For this motor operating principle, a two-dimensional extensional standing wave is stimulated in the piezoelectric plate to achieve the slope-line elliptical motion of its driving tip. Based on the internal coupling effect caused by the crystal anisotropy, Tamura et al. [11] designed a thin-plate piezoelectric transducer to be the stator of an ultrasonic motor. A coupling vibration mode was excited in a $LiNbO_3$ rectangular plate vibrator to achieve the miniature single-phase drive ultrasonic motor. He et al. [12] presented a tubular ultrasonic motor that only uses a single vibration bending mode of a piezoelectric tube to produce rotation motion. The piezoelectric tube is only excited by one driving signal, and no vibration mode coupling is required. Yokoyama et al. [13] developed a linear ultrasonic motor using a single resonance mode driven by a single excitation signal, in which two square plates linked by V-shaped beams are employed as the motor stator. Liu et al. [14] designed a sandwich plated piezoelectric transducer with single vibration mode, producing slash elliptical motion at its driving tip to push a slider for constructing a linear ultrasonic motor. Chang et al. [15] proposed a screw-thread-type ultrasonic motor with single-phase excitation by designing an asymmetrical piezoelectric transducer to generate two orthogonal bending vibration modes. Based on the structural properties of the transducer, Ma et al. [16–19] developed standing wave piezoelectric transducers with single phase excitation for pushing a rotor/slider to achieve ultrasonic motors, respectively. Most aforementioned piezoelectric transducers are designed as the standing wave vibrator for ultrasonic motors. However, the wear problem is hard to avoid for standing wave ultrasonic motors due to the limited contact area between their stator and slider/rotor. It has been demonstrated that traveling wave ultrasonic motors are the cost-efficient, durable and stable actuator during industrial applications due to the large contact area between the stator and the rotor during operation.

Therefore, inspired by the transducer design method in Refs. [9–19], a novel traveling wave sandwich piezoelectric transducer with single phase excitation is proposed in this study. Only one excitation signal is required to apply to the transducer, and traveling waves with the same rotational direction are produced in two driving rings utilizing the structural coupling property of a beam-ring combined element. This is done in order to achieve elliptical motion of surface points of the two driving rings, largely simplifying the control system. A pre-tensioning mechanism is designed to mount four groups of complete lead zirconate titanate piezoelectric ceramic (PZT) elements by one bolt, avoiding the unequal pre-stresses issue of all PZT elements.

This paper is organized as follows. Initially, the configuration and operating principle of the proposed transducer are explained in detailed. Subsequently, an analytical model is developed utilizing the transfer matrix method (TMM) to study the dynamic behavior of the proposed transducer. In addition, experimental validation is conducted in order to validate the feasibility of the developed transfer matrix model and to confirm the operating principle and design of the proposed transducer. Moreover, motion trajectory of surface points and quality of the driving ring are calculated based on the developed model to study the driving concept of the transducer. Application example of the proposed transducer is then investigated to evaluate the driving performance of the

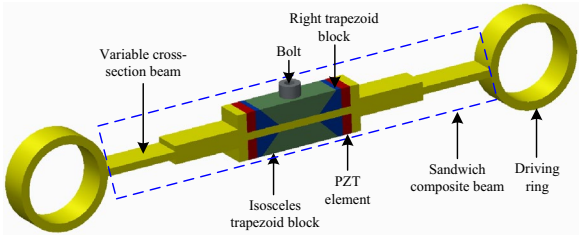

Figure 1 Three-dimensional view of the proposed traveling wave sandwich piezoelectric transducer

proposed transducer prototype. Finally, a conclusion is presented.

2 Structure Design and Operating Principle

2.1 Structure Design

The three-dimensional view of the proposed traveling wave sandwich piezoelectric transducer excited by a single-phase signal is illustrated in Figure 1. It is composed of a sandwich composite beam and two driving rings. The sandwich composite beam is comprised of a variable cross-section beam, a pre-tensioning mechanism, and four groups of PZT elements. The pre-tensioning mechanism consists of two isosceles trapezoid blocks, four right trapezoid blocks, and a bolt. Each PZT element is polarized along its thickness direction, and two pieces of complete and rectangular PZT elements with opposite polarization directions form a group of excitation unit. One isosceles trapezoid block and two right trapezoid blocks form a rectangular block. Therefore, the pre-tensioning mechanism is comprised of two rectangular blocks and a bolt. The middle of the variable cross-section beam is designed with two rectangular grooves at its upper and lower surfaces. A rectangular block and two groups of PZT elements placed at its both ends are combined together to fill into one rectangular groove. Therefore, the two isosceles trapezoid blocks are connected by the bolt, ensuring the pre-tensioning mechanism and the four groups of PZT elements are mounted in the variable cross-section beam. This ensures that all the PZT elements are applied with equal pre-stress. The two driving rings are placed at both ends of the sandwich composite beam.

2.2 Operating Principle

In order to achieve the drive function, elliptical motion is required to be produced at surface points of the two driving rings. As an electrical signal is simultaneously applied to all the PZT elements, the sandwich composite beam is excited to vibrate at the first order longitudinal vibration, and two driving rings are simultaneously stimulated to vibrate at a third order in-plane radial bending vibration, as shown in Figure 2(a). The aforementioned two vibrations are the natural vibration mode of the driving ring and sandwich composite beam. Once the resonant frequencies of the two vibrations are close or the same, they will be stimulated in the ring-beam composite structure under the external forced excitation. This is the reason why the first order longitudinal vibration and the third order in-plane radial bending vibration can be simultaneously excited in the transducer under a single-phase signal. Therefore, a periodical movement of each surface point of the driving ring along its radial direction is achieved. It should be pointed out that the two third order in-plane bending vibrations of the two driving rings have a spatial phase difference of π. Due to the structural coupling between the sandwich composite beam and two driving rings, the sixth order bending vibration is induced in the sandwich composite beam, and another third order in-plane bending vibration is produced in the driving ring along the tangential direction as well, as shown in Figure 2(b). Since the longitudinal vibration of the sandwich composite beam has two mechanical parameters (longitudinal force F and longitudinal velocity v),

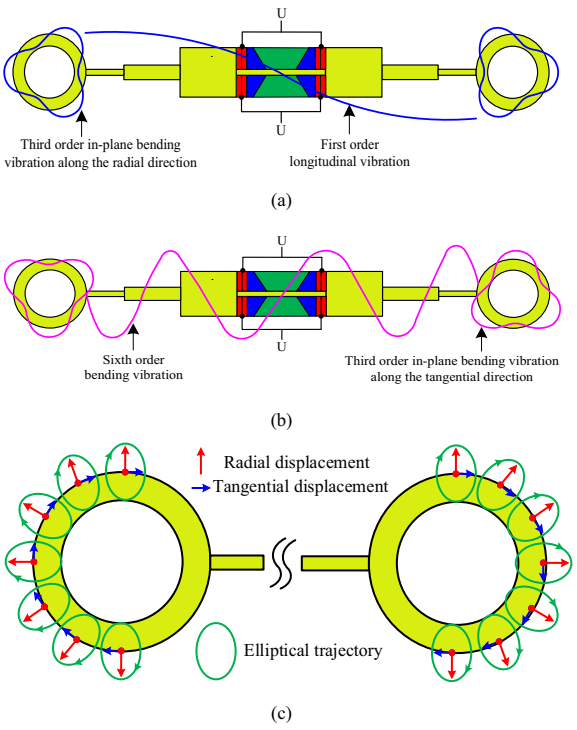

Figure 2 Operating principle of the proposed traveling wave sandwich piezoelectric transducer: **a** Vibration mode of the proposed transducer with a single-phase excitation, **b** Induced vibration of the proposed transducer due to the structural coupling between the sandwich composite beam and driving rings, **c** Elliptical trajectories produced on the surface points of the two driving rings

whereas the in-plane bending vibration of the ring holds six mechanical parameters (radial force Q_R, tensile force N, bending moment M, radial displacement u, tangential displacement Ω, and rotational slope ψ), it cannot meet the rules of force balance and equal velocity at the connecting interface between the ring and beam. Therefore, it will be an unbalance state at the connection interface. In order to keep a balance state, another four mechanical parameters (shear velocity w, angular velocity $\dot{\psi}$, bending moment M, and shear force Q) should be included in the sandwich composite beam. This means that the bending vibration is induced in the sandwich composite beam. Meanwhile, due to the existence of the four shear mechanical parameters (tensile force N, bending moment M, radial displacement u, tangential displacement Ω, and rotational slope ψ), the in-plane tangential bending vibration is also induced in the driving rings. The two third order in-plane bending vibrations produced in each driving ring along the radial and tangential directions, respectively, have a spatial phase difference of π/2, leading to the generation of traveling wave in each driving ring. For each surface point, its movements are occurred in the radial and tangential directions of the driving ring in the same time. This results in the generation of elliptical motion of the driving rings. As the two induced third order in-plane bending vibrations of the two driving rings along the tangential direction have a spatial phase difference of π, the traveling waves produced in the two driving rings rotate the same direction. Therefore, surface points of the driving rings move in elliptical motion with the same direction, as shown in Figure 2(c).

3 Analytical Modelling

To further understand the operating principle and analyze the dynamic behavior of the proposed transducer, an analytical model is developed using the TMM in Section 3. Compared to other analytical solutions, the TMM minimizes the computational effort and provides a precise solution. Using the TMM, a complex system can be divided into many simple and continuous elements, such as beams, rods, or plates [20–22]. Then the independent transfer matrix model can be described for each element according to the basic wave motion equations and the arbitrary harmonic boundary conditions [23]. Through transfer conditions, the overall transfer matrix model of the entire system can be calculated by combining the independent transfer matrices of all discrete elements. Applying boundary conditions of the system, a linear equation set can be obtained and solved to describe the dynamic behavior of the complex system. For the PZT element, the mechanical and electrical properties can be simultaneously considered in its transfer matrix model [24], making the TMM suitable for the analysis of piezoelectric transducers.

The discrete model of the proposed sandwich piezoelectric transducer is shown in Figure 3. The transducer is divided into eleven elements, including two curved elastic beams, seven elastic beams, and two sandwich beams. The sandwich beam is composed of an elastic beam and two groups of PZT elements located on the upper and lower surfaces of the elastic beam, respectively. As the four groups of PZT elements are excited to vibrate at the longitudinal vibration, the seven elastic beams and two sandwich beams are subjected to this vibration and the bending vibration induced by the structural coupling of the sandwich composite beam and driving ring. Therefore, the longitudinal and bending vibration transfer matrix models should be created for these beam elements. As the two curved beams are excited at the in-plane bending vibration, the corresponding transfer matrix model should be carried out. In the following sections, the aforementioned transfer matrix model of each discrete element will be given and explained in detail.

3.1 Longitudinal Vibration Modelling

Longitudinal vibration is the major vibration stimulated in the sandwich composite beam, therefore, the transfer matrix model of each discrete element in this beam must first be developed. In Refs. [23, 25, 26], the longitudinal vibration transfer matrix model of the elastic beam has been presented as

$$\begin{bmatrix} v_{ir} \\ F_{ir} \end{bmatrix} = \boldsymbol{T_{iL}} \begin{bmatrix} v_{il} \\ F_{il} \end{bmatrix} = \begin{bmatrix} T_{iL,11} & T_{iL,12} \\ T_{iL,21} & T_{iL,22} \end{bmatrix} \begin{bmatrix} v_{il} \\ F_{il} \end{bmatrix}, \tag{1}$$

where v_{il} and v_{ir} are the left and right velocities of the elastic beam i, respectively; F_{il} and F_{ir} are the left and right forces of the elastic beam i, respectively, and $\boldsymbol{T_{iL}}$ is the longitudinal vibration transfer matrix with following components: $T_{iL,11} = \cos(k_i l_i)$, $T_{iL,12} = \frac{j}{z_i}\sin(k_i l_i)$, $T_{iL,21} = jz_i \sin(k_i l_i)$, and $T_{iL,22} = \cos(k_i l_i)$, in which $z_i = A_i\sqrt{\rho_i E_i}$ is the impedance, $k_i = \omega/c_i$ is the wave number; $c_i = \sqrt{E_i/\rho_i}$ is the wave velocity, ω is the angular frequency; A_i is the cross-section area; E_i and ρ_i are

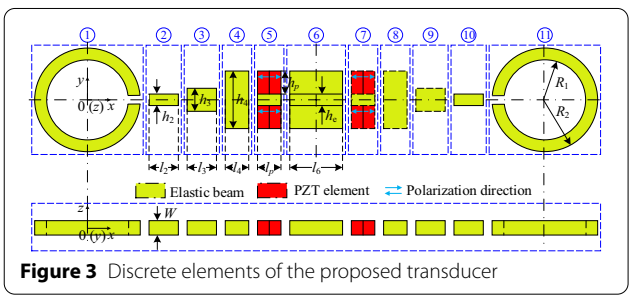

Figure 3 Discrete elements of the proposed transducer

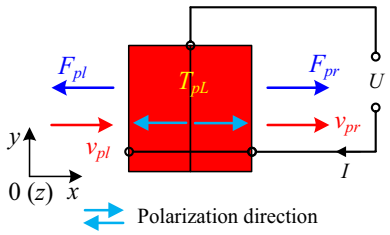

Figure 4 Transfer matrix model of a group of PZT elements

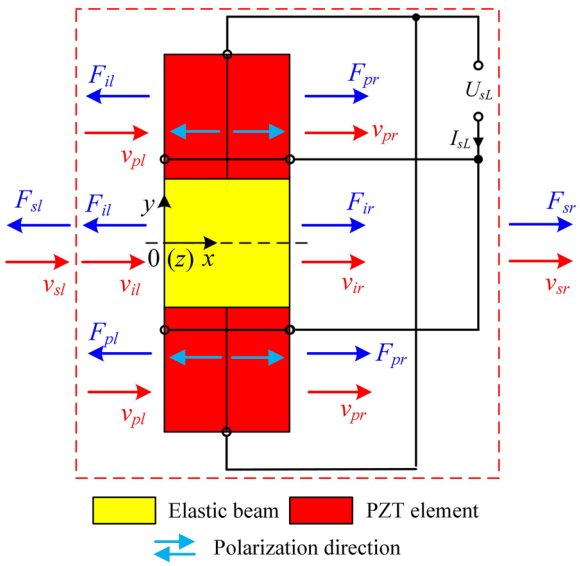

Figure 5 Transfer matrix model of the sandwich beam for longitudinal vibration [24]

the Young's modulus and density of the elastic beam i, respectively; and l_i is the length of the elastic beam i (The subscript i is the number of the discrete element, in which $i \in [1\ 11]$ (i.e., i belongs to the interval 1 to 11)).

Due to the fact that each group of PZT elements operates at their d_{33} vibration mode to produce the longitudinal vibration, its transfer matrix model (see in Figure 4) must simultaneously include the mechanical and electrical coupling properties [23–26], as written:

$$\begin{bmatrix} v_{pr} \\ F_{pr} \\ I \end{bmatrix} = \boldsymbol{T_{pL}} \begin{bmatrix} v_{pl} \\ F_{pl} \\ U \end{bmatrix} = \begin{bmatrix} T_{pL,11} & T_{pL,12} & T_{pL,13} \\ T_{pL,21} & T_{pL,22} & T_{pL,23} \\ T_{pL,31} & T_{pL,\mathbf{32}} & T_{pL,\mathbf{33}} \end{bmatrix} \begin{bmatrix} v_{pl} \\ F_{pl} \\ U \end{bmatrix}, \tag{2}$$

where $()_{pl}$ and $()_{pr}$ are the parameters (force and velocity) of the two ends of the group of PZT elements, respectively; U and I are the input voltage and induced current of the group of PZT elements, respectively, and $\boldsymbol{T_{pL}}$ denotes the transfer matrix of the group of PZT elements operating in the d_{33} vibration mode, in which its matrix components are expressed as follows: $T_{pL,11} = \cos(k_p l_p)$, $T_{pL,12} = \frac{j}{A_p z_p}\sin(k_p l_p)$, $T_{pL,13} = \frac{j\alpha_p}{A_p z_p}\sin(k_p l_p)$, $T_{pL,21} = jA_p z_p \sin(k_p l_p)$, $T_{pL,22} = T_{pL,11}$, $T_{pL,23} = \alpha_p(\cos(k_p l_p) - 1)$, $T_{pL,31} = T_{pL,23}$, $T_{pL,32} = T_{pL,13}$, and $T_{pL,33} = j\omega C_{0p} +$ $T_{pL,33} = j\omega C_{0p} + \frac{j\alpha_p^2}{A_p z_p}\sin(k_p l_p)$, where $k_p = \omega/c_i$ is the wave number, $z_p = 1/(c_p s_{33}^E)$ the impedance, $c_p = 1/\sqrt{\rho_p s_{33}^E}$ the wave velocity, $C_{0p} = \frac{4A_p}{l_p}(\varepsilon_{33}^T - \frac{d_{33}^2}{s_{33}^E})$, and $\alpha_p = \frac{2A_p d_{33}}{s_{33}^E l_p}$ the electromechanical translation factor of the PZT element, in which s_{33}^E represents the compliance parameter, ε_{33}^E denotes the dielectric coefficients, d_{33} denotes the piezoelectric strain coefficients, ρ_p denotes the density, l_p is the total length of a group of PZT elements, and A_p is the cross-section area of the PZT element.

For the sandwich beam, its transfer matrix model in longitudinal vibration can be described by combining the transfer matrices of the elastic beam and the two group of PZT elements and considering the boundary conditions, as shown in Figure 5. In Ref. [26], the coupling longitudinal vibration transfer matrix model was developed and expressed as:

$$\begin{bmatrix} v_{sr} \\ F_{sr} \\ I_{sL} \end{bmatrix} = \boldsymbol{T_{sL}} \begin{bmatrix} v_{sl} \\ F_{sl} \\ U_{sL} \end{bmatrix} = \begin{bmatrix} T_{sL,11} & T_{sL,12} & T_{sL,13} \\ T_{sL,21} & T_{sL,22} & T_{sL,\mathbf{23}} \\ T_{sL,\mathbf{31}} & T_{sL,\mathbf{32}} & T_{sL,\mathbf{33}} \end{bmatrix} \begin{bmatrix} v_{sl} \\ F_{sl} \\ U_{sL} \end{bmatrix}, \tag{3}$$

where $()_{sl}$ and $()_{sr}$ are the parameters (force and velocity) of the left and right ends of the sandwich beam, respectively; U_{sL} and I_{sL} are the input voltage and induced current of the sandwich beam, respectively; $\boldsymbol{T_{sL}}$ is the longitudinal vibration transfer matrix of the sandwich beam and the detailed expression of its matrix components can be found in Appendix A.

3.2 Bending Vibration Modelling

Due to the structural coupling of the sandwich composite beam and driving rings, all discrete elements in the sandwich composite beam are induced to present bending vibration. According to the geometrical property of the elastic beam, its bending vibration can be formulated using the Timoshenko beam theory by considering the rotary inertia and shear deformation, which has been reported by Pestel et al. [20], written as

$$\begin{bmatrix} w_{ir} \\ \dot{\psi}_{ir} \\ M_{ir} \\ Q_{ir} \end{bmatrix} = \boldsymbol{T_{iB}} \begin{bmatrix} w_{il} \\ \dot{\psi}_{il} \\ M_{il} \\ Q_{il} \end{bmatrix} = \begin{bmatrix} T_{iB,11} & T_{iB,12} & T_{iB,13} & T_{iB,14} \\ T_{iB,21} & T_{iB,22} & T_{iB,23} & T_{iB,24} \\ T_{iB,31} & T_{iB,32} & T_{iB,33} & T_{iB,34} \\ T_{iB,41} & T_{iB,42} & T_{iB,43} & T_{iB,44} \end{bmatrix} \begin{bmatrix} w_{il} \\ \dot{\psi}_{il} \\ M_{il} \\ Q_{il} \end{bmatrix}, \tag{4}$$

where shear velocity w, angular velocity $\dot{\psi}$, bending moment M, and shear force Q are the mechanical parameters to describe the bending vibration of the elastic beam, and $\boldsymbol{T_{iB}}$ is the bending vibration transfer matrix of the elastic beam, in which its matrix components can be found in the Appendix B.

For the sandwich beam, the two groups of PZT elements are subjected with the same bending vibration as elastic beams, meaning that the electric parameters do not involve in the bending vibration. Therefore, the expression of the bending vibration transfer matrix model of the sandwich beam should be described the same as that of the elastic beam:

$$\begin{bmatrix} w_{sr} \\ \dot{\psi}_{sr} \\ M_{sr} \\ Q_{sr} \end{bmatrix} = \boldsymbol{T_{sB}} \begin{bmatrix} w_{sl} \\ \dot{\psi}_{sl} \\ M_{sl} \\ Q_{sl} \end{bmatrix}, \tag{5}$$

where $\boldsymbol{T}_{sB}$ is the bending vibration transfer matrix of the sandwich beam with the substitutions of $\sigma_s = \frac{\mu_s \omega^2}{(GA)_s} l_p^2$, $\tau_s = \frac{(\rho I)_s \omega^2}{(EI)_s} l_p^2$, $\beta_s^4 = \frac{\mu_s \omega^2}{(EI)_s} l_p^4$, $a_s = \frac{l_p^2}{(EI)_s}$, and

$$\begin{cases} (GA)_s = \kappa^2 W \left(h_e G_e + \frac{2h_p}{s_{55}^E} \right) \\ (EI)_s = \frac{h_e^3 W E_e}{12} + \frac{2W}{3 s_{33}^E} \left(\left(\frac{h_e}{2} + h_p \right)^3 - \left(\frac{h_e}{2} \right)^3 \right) \\ (\rho I)_s = \frac{\rho_e W h_e^3}{12} + \frac{2}{3} \rho_p W \left(\left(\frac{h_e}{2} + h_p \right)^3 - \left(\frac{h_e}{2} \right)^3 \right) \\ \mu_s = \rho_e W h_e + 2 \rho_p W h_p \end{cases}, \quad \text{in}$$

which e is the element number 5 or 7, h_p is the height of the PZT element, and s_{55}^E is the shear compliance parameter of the PZT element.

The curved beams are excited to vibrate at the third order in-plane bending vibration. Therefore, their transfer matrix models should consider six mechanical parameters, including radial force Q_R, tensile force N, bending moment M, radial displacement u, tangential displacement Ω, and rotational slope ψ. By solving the governing equations of the in-plane bending vibration, Irie et al. [27] calculated the coefficient matrix $\boldsymbol{H}$, written as:

$$\boldsymbol{H} = \begin{bmatrix} 0 & \frac{R}{\kappa_c A_c G_c} & -1 & R & 0 & 0 \\ -n(1+k^2) & 0 & 0 & 0 & 0 & -1 \\ 1 & 0 & 0 & 0 & 0 & \frac{R}{E_c A_c} \\ 0 & 0 & 0 & 0 & \frac{1}{E_c A_c R k^2} & 0 \\ 0 & -R & -nRk_1^2 & -nR^2 k_2^2 & 0 & 0 \\ 0 & 1 & -n(1+k^2) & -nRk_1^2 & 0 & 0 \end{bmatrix}, \tag{6}$$

where c is the curved beam number 1 or 11; $R = (R_1+R_2)/2$ is the radius in the neutral axis of the curved beam while its outer and inner radii are denoted as R_1 and R_2, respectively; the quantities k^2, k_1^2 and k_2^2 are the dimensionless parameters, and $n = \rho_c A_c R \omega^2$.

Therefore, the transfer matrix model of the curved beam with the in-plane bending vibration can be formulated as:

$$\boldsymbol{Z_b} = \boldsymbol{T_c}(\theta) \boldsymbol{Z_a} = \exp(H\theta) \boldsymbol{Z_a}, \tag{7}$$

where $\boldsymbol{Z_a} = [u_a \ Q_{Ra} \ \Omega_a \ \psi_a \ M_a \ N_a]^{\mathrm{T}}$ and $\boldsymbol{Z_b} = [u_b \ Q_{Rb} \ \Omega_b \ \psi_b \ M_b \ N_b]^{\mathrm{T}}$ are the state vectors of both ends of the curved beam, respectively, and $\boldsymbol{T_c}(\theta) = \exp(H\theta)$ is the transfer matrix with the dimension of 6×6 as the curved beam is with the angle θ.

The state vector of the curved beam includes the force and displacement parameters, while that of its neighbouring elastic beam contains the force and velocity parameters. Therefore, to achieve the matching of the state vectors between the elastic beam and curved beam, the displacement parameters of the curved beam should be converted as the velocity parameters according to the formulation of $u = j\omega v$. The new expression of the transfer matrix model of the curved beam can be written as

$$\boldsymbol{Z'_b} = \boldsymbol{T'_c}(\theta) \boldsymbol{Z'_a}, \tag{8}$$

where $\boldsymbol{Z'_a} = [v_a \ \ Q_{Ra} \ \ w_a \ \ \dot{\psi}_a \ \ M_a \ \ N_a]^{\mathrm{T}}$ and $\boldsymbol{Z'_b} = [v_b \ \ Q_{Rb} \ \ w_b \ \ \dot{\psi}_b \ \ M_b \ \ N_b]^{\mathrm{T}}$ are the input and output state vectors of the curved beam containing the force and velocity parameters, and $\boldsymbol{T'_c}(\boldsymbol{\theta})$ is the new expression of the in-plane beading vibration transfer matrix of the curved beam.

3.3 Damping Characteristic

The damping effect of the real material has a substantial influence on the output performance of the proposed transducer and should therefore be considered in the transfer matrix model developed here. As reported in Ref. [28], the damping effect can be described by the complex Young's modulus $\underline{E}_i = E_i(1 + j\frac{1}{\zeta_i})$ for general materials, and the complex compliance coefficient $\underline{S}_{33}^E = S_{33}^E/(1 + j\frac{1}{\zeta_p})$ for the PZT element, in which ζ_i and ζ_p are the quality factors of the general material and the PZT element, respectively. Due to the specific material

properties of the PZT element, its damping effect still includes the dielectric and piezoelectric losses. These two losses can be presented by a complex dielectric constant $\underline{\varepsilon}_{33}^{T}$ and a complex piezoelectric constant $\underline{d}_{33}$, as formulated

$$\underline{\varepsilon}_{33}^{T} = \varepsilon_{33}^{T}[1 + j\tan(\delta)], \tag{9}$$

$$\underline{d}_{33} = d_{33}[1 + j\tan(\eta)], \tag{10}$$

with the dissipation factors $\tan(\delta)$ and $\tan(\eta)$ for the dielectric loss and piezoelectric loss, respectively.

3.4 Transfer Matrix Model of Combined Vibrations

As the longitudinal and bending vibrations are simultaneously generated in the sandwich composite beam, a total transfer matrix model used to describe these two vibrations together should be developed to simplify the final analytical model. The combined transfer matrix model for the elastic beam can be formulated as

$$\boldsymbol{Z_{ir}} = \boldsymbol{T}_i\boldsymbol{Z_{il}} = \begin{bmatrix} T_{iL} & 0 \\ 0 & T_{iB} \end{bmatrix}\boldsymbol{Z_{il}}, \tag{11}$$

where $\boldsymbol{Z_{il}} = \left[\, v_{il}\ F_{il}\ w_{il}\ \dot{\psi}_{il}\ M_{il}\ Q_{il} \,\right]^{\mathrm{T}}$ and $\boldsymbol{Z_{ir}} = \left[\, v_{ir}\ F_{ir}\ w_{ir}\ \dot{\psi}_{ir}\ M_{ir}\ Q_{ir} \,\right]^{\mathrm{T}}$ are the input and output state vectors of the elastic beam i, including all mechanical parameters for describing the longitudinal and bending vibrations, respectively, and T_i is the combined transfer matrix with the dimension of 6×6 for the elastic beam i.

Combining Eqs. (3) and (5), the total transfer matrix model of the sandwich beam is expressed as

$$\boldsymbol{Z_{sr}} = \boldsymbol{T}_s\boldsymbol{Z_{sl}} = \begin{bmatrix} \boldsymbol{T_{sL}} & 0 \\ 0 & \boldsymbol{T_{sB}} \end{bmatrix}\boldsymbol{Z_{sl}}, \tag{12}$$

where $\boldsymbol{Z_{sl}} = \left[\, v_{sl}\ F_{sl}\ U_{sL}\ w_{sl}\ \dot{\psi}_{sl}\ M_{sl}\ Q_{sl} \,\right]^{T}$ and $\boldsymbol{Z_{sr}} = \left[\, v_{sr}\ F_{sr}\ I_{sL}\ w_{sr}\ \dot{\psi}_{sr}\ M_{sr}\ Q_{sr} \,\right]^{T}$ are input and output state vectors of the sandwich beam containing mechanical and electrical parameters of the two vibrations, respectively, and $\boldsymbol{T_s}$ is the total transfer matrix with the dimension of 7×7 for the sandwich beam.

3.5 Transfer Conditions

In order to combine all the discrete elements, transfer conditions between two neighbouring elements should be analyzed by following the rules of force balance and equal velocity at the connecting interface. In our proposed transducer, five kinds of transfer conditions exist. The first transfer condition is defined that the vibration is transferred from the left curved beam 1 to the neighbouring elastic beam 2, which can be formulated as

$$\begin{cases} \boldsymbol{C_1Z_1} + \boldsymbol{C_2Z_2} - \boldsymbol{Z_3} = 0, \\ \boldsymbol{C_3Z_1} - \boldsymbol{C_3Z_2} = 0, \end{cases} \tag{13}$$

where $\boldsymbol{C}_1$, $\boldsymbol{C}_2$, and $\boldsymbol{C}_3$ are the transfer condition matrices with the dimension of 6×6; $\boldsymbol{Z}_1$=[v_1 Q_{R1} w_1 $\dot{\psi}_1$ M_1 N_1]$^{\mathrm{T}}$ and $\boldsymbol{Z}_2$=[v_2 Q_{R2} w_2 $\dot{\psi}_2$ M_2 N_2]$^{\mathrm{T}}$ are the input and output state vectors of the curved beam 1, respectively; $\boldsymbol{Z_3} = \left[\, v_3\ F_3\ w_3\ \dot{\psi}_3\ M_3\ Q_3 \,\right]^{\mathrm{T}}$ is the input state vector of the elastic beam 2.

The second transfer condition is used to describe the connection between two neighbouring elastic beams i and i+1, which can be written as:

$$\boldsymbol{C_u}\boldsymbol{Z_{2i}} - \boldsymbol{Z_{2i+1}} = 0, \tag{14}$$

where the transfer condition matrix $\boldsymbol{C_u}$ is a unit matrix with the dimension of 6×6, $\boldsymbol{Z_{2i}} = \left[\, v_{2i}\ F_{2i}\ w_{2i}\ \dot{\psi}_{2i}\ M_{2i}\ Q_{2i} \,\right]^{\mathrm{T}}$ and $\boldsymbol{Z_{2i+1}} = \left[\, v_{2i+1}\ F_{2i+1}\ w_{2i+1}\ \dot{\psi}_{2i+1}\ M_{2i+1}\ Q_{2i+1} \,\right]^{\mathrm{T}}$ are the output and input state vectors of the elastic beam i and i+1, respectively.

The third kind of transfer condition is that the transmission of the vibration is from the elastic beam i to the sandwich beam. Due to the unequal dimension of their state vectors, this transfer condition should be formulated as:

$$\boldsymbol{C_u}\boldsymbol{Z_{2i}} - \boldsymbol{C_4}\boldsymbol{Z_{sl}} = 0, \tag{15}$$

where $\boldsymbol{C}_4$ is the transfer condition matrix with the dimension of 7×7.

The fourth kind of transfer condition is defined as the vibration that is transferred from the sandwich beam to the neighboring elastic beam i. In this case, the transfer condition should be described as

$$\boldsymbol{C_4}\boldsymbol{Z_{sr}} - \boldsymbol{C_u}\boldsymbol{Z_{2i-1}} = 0, \tag{16}$$

where $\boldsymbol{Z_{2i-1}} = \left[\, v_{2i-1}\ F_{2i-1}\ w_{2i-1}\ \dot{\psi}_{2i-1}\ M_{2i-1}\ Q_{2i-1} \,\right]^{\mathrm{T}}$ is the input state vector of the elastic beam i.

The last transfer condition is that the vibration transfers from the elastic beam 10 to the right curved beam, which is written as:

$$\begin{cases} \boldsymbol{C_5Z_{21}} + \boldsymbol{C_6Z_{22}} - \boldsymbol{Z_{20}} = 0, \\ \boldsymbol{C_3Z_{21}} - \boldsymbol{C_3Z_{22}} = 0, \end{cases} \tag{17}$$

where $\boldsymbol{C_5}$ and $\boldsymbol{C_6}$ are the transfer condition matrices with the dimension of 6×6, $\boldsymbol{Z_{20}} = \left[\, v_{20}\ F_{20}\ w_{20}\ \dot{\psi}_{20}\ M_{20}\ Q_{20} \,\right]^{\mathrm{T}}$ is the output state vector of the elastic beam 10, $\boldsymbol{Z}_{21}$ = [v_{21} Q_{R21} w_{21} $\dot{\psi}_{21}$ M_{21} N_{21}]$^{\mathrm{T}}$ and $\boldsymbol{Z}_{22}$ = [v_{22} Q_{R22} w_{22} $\dot{\psi}_{22}$ M_{22} N_{22}]$^{\mathrm{T}}$ are the input and output state vectors of the curved beam 11, respectively.

Using the aforementioned five kinds of transfer conditions, all the discrete elements can be physically combined together.

3.6 Overall Transfer Matrix Model

Combining all independent transfer matrices of the divided elements, transfer conditions, and boundary conditions, the overall transfer matrix model of the proposed transducer is formulated as Eq. (18).

In this overall transfer matrix model, $\boldsymbol{S_m}$ is the systematic matrix, including total physical transfer matrix $\boldsymbol{T_{pm}}$, total transfer condition matrix $\boldsymbol{C_m}$, and total boundary condition extraction matrix $\boldsymbol{B_m}$, $\boldsymbol{Z_m}$ is the state vector containing all input and output parameters, and $\boldsymbol{A_m}$ is the total electrical excitation conditions, as the entire transducer is a closed system without any mechanical boundary conditions. In the total boundary condition extraction matrix $\boldsymbol{B_m}$, the matrix $\boldsymbol{B}$ with the dimension of 1×7 is used to extract the excitation voltage U_{sL} applied to the sandwich beam. Therefore, the corresponding value of the extracted excitation voltage is expressed by the matrix $\boldsymbol{A}$ with the dimension of 1×1. It can be noted that the total transfer matrix model the proposed transducer is a linear equation set, which can be easily solved using the Matlab software. Thus, the dynamic behavior of the transducer can be calculated by solving the developed transfer matrix model.

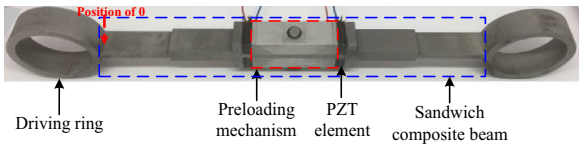

Figure 6 Prototype of the traveling wave sandwich piezoelectric transducer

4 Experimental Validation

To validate the effectiveness of the developed transfer matrix model and to confirm the feasibility of the design and operating principle of the proposed transducer, we first manufactured and assembled the prototype of the transducer and then conducted vibration measurements. The prototype of the proposed transducer with a weight of 225 g is depicted in Figure 6, and its geometrical sizes are listed in Table 1. All elastic beams and curved elastic beams were made of stainless steel, and the PZT element was made of PIC-181 type piezoelectric ceramic (PI Company, Germany). The material parameters of the transducer prototype are listed in Table 2.

$$
\begin{bmatrix} T_{pm} \\ C_m \\ B_m \end{bmatrix}_{S_m} \begin{bmatrix} Z_1 \\ Z_2 \\ Z_3 \\ Z_4 \\ Z_5 \\ Z_6 \\ Z_7 \\ Z_8 \\ Z_9 \\ Z_{10} \\ Z_{11} \\ Z_{12} \\ Z_{13} \\ Z_{14} \\ Z_{15} \\ Z_{16} \\ Z_{17} \\ Z_{18} \\ Z_{19} \\ Z_{20} \\ Z_{21} \\ Z_{22} \end{bmatrix}_{Z_m} = \begin{bmatrix} 0 \\ 0 \\ 0 \\ 0 \\ 0 \\ 0 \\ 0 \\ 0 \\ 0 \\ 0 \\ 0 \\ 0 \\ 0 \\ 0 \\ 0 \\ 0 \\ 0 \\ 0 \\ 0 \\ 0 \\ A \\ A \end{bmatrix}_{A_m}, \tag{18}
$$

Table 1 Geometrical sizes of the proposed transducer prototype (mm)

Sizes	R_1	R_2	l_2	l_3	l_4	l_p	l_6	h_2	h_3	h_4	h_e	h_p	W
Value	15.75	19.25	30	28	4	4	38	3	7.5	19	3	8	12

Table 2 Material parameters of the proposed transducer prototype

Parameters	Stainless steel	PIC-181
Density (kg/m^3)	7750	7850
Young's modulus (GPa)	190	$\begin{pmatrix} 152 & 891 & 855 & 0 & 0 & 0 \\ 891 & 152 & 855 & 0 & 0 & 0 \\ 855 & 855 & 131 & 0 & 0 & 0 \\ 0 & 0 & 0 & 316 & 0 & 0 \\ 0 & 0 & 0 & 0 & 283 & 0 \\ 0 & 0 & 0 & 0 & 0 & 283 \end{pmatrix}$
Poisson' ratio	0.31	/
Piezoelectric constant (C/m^2)	/	$\begin{pmatrix} 0 & 0 & -4.44 \\ 0 & 0 & -4.44 \\ 0 & 0 & 14.78 \\ 0 & 11.01 & 0 \\ 11.01 & 0 & 0 \\ 0 & 0 & 0 \end{pmatrix}$

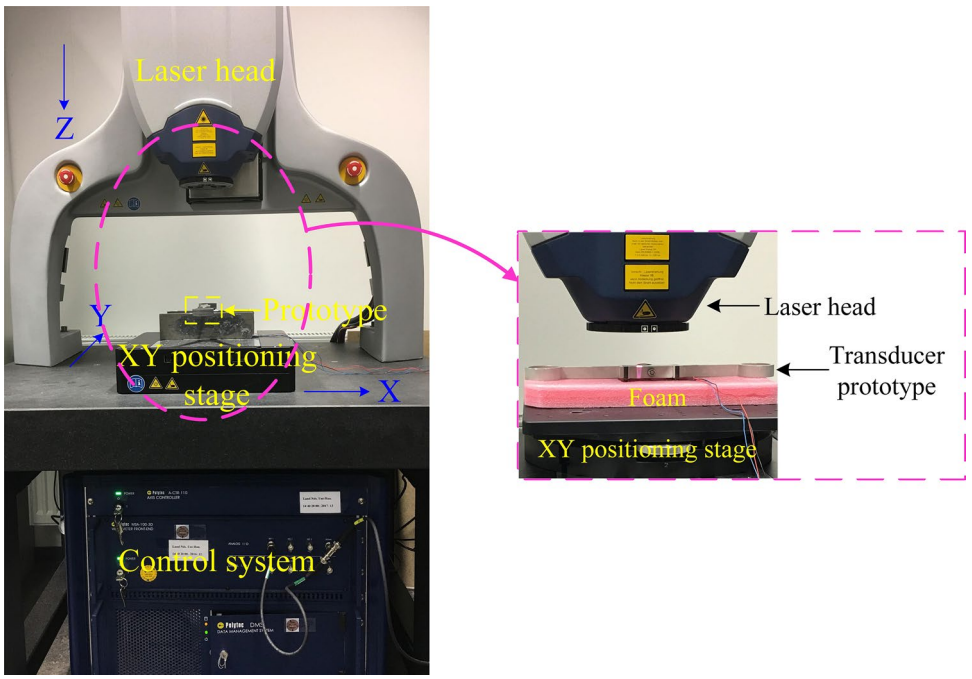

Figure 7 Experimental system for measuring the three-dimensional vibration characteristics of the transducer prototype

An experimental system was built up to measure three-dimensional vibration characteristics of the transducer prototype, as shown in Figure 7. The major component of the experimental system is a 3D laser Doppler vibrometer (MSA-100-3D, Polytec, Germany), which is composed of a control system, a *XY* positioning stage, and a laser head. The control system is used to analyze and process the measured data. The laser head is adopted to emit three laser beams, and it can move up and down in the *Z* direction. Additionally, the transducer prototype was placed on the *XY* positioning stage, and a foam was located between the transducer prototype and the *XY* positioning stage in order to keep the free boundary conditions of the transducer prototype. Therefore, the experimental system enabled us to measure the three-dimensional vibration characteristics of the transducer prototype.

4.1 Frequency Response Characteristic

The frequency response characteristic of the transducer prototype was initially measured to obtain the resonant frequency of the operating vibration mode. The measured frequency swept from 19 kHz to 20 kHz with an interval of 1 Hz while the excitation voltage was 1 V. The connection position between the sandwich composite beam and left driving ring was tested to obtain the frequency response characteristic of the transducer prototype, and the result was plotted in Figure 8, leaving a resonant frequency of 19392 Hz. Under the same excitation conditions, the frequency response characteristic was calculated by the developed transfer matrix model (Eq. (18)), as also illustrated in Figure 8. The amplitudes (u_{left} and u_{right}) of both ends of the sandwich composite beam were computed to exhibit the frequency response characteristic of the transducer. It can be noted that the calculated resonant frequency of the operating vibration mode is 19821 Hz for the transducer, showing a frequency difference of 429 Hz compared to the experimental results. The difference between the calculated and measured resonant frequencies is mainly due to the fact that our developed analytical model does not consider the influence of pre-stress applied on the PZT elements during assembly. The comparison still demonstrated the feasibility of the created transfer matrix model and confirmed the validation of the operating principle of the proposed transducer.

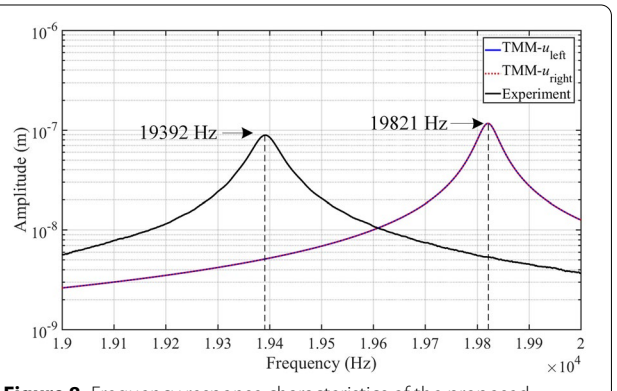

Figure 8 Frequency response characteristics of the proposed piezoelectric transducer calculated by TMM and measured by experiments

4.2 Vibration Shapes

At the measured resonant frequency of 19392 Hz, the vibration shapes of the left driving ring and the sandwich composite beam were measured with the excitation voltage of 2 V using the aforementioned experimental system, as illustrated in Figure 9. To further validate the developed transfer matrix model, the vibration shapes of the transducer were computed and compared to the experimental results in Figure 9. The calculated vibration shapes were computed at the calculated resonant frequency of 19821 Hz. The measured and computed first order longitudinal vibration shapes of the sandwich composite beam presented in Figure 9(a) showed good agreement with each other. Due to the structural coupling between the sandwich composite beam and the left driving ring, the sixth order bending vibration was induced in the composited beam, as illustrated in Figure 9(b). It can be seen that the computed bending vibration shape matches well with the experimental result. In Figure 9(c), the radial and tangential displacements of each point in the left driving ring are calculated and exhibit the in-plane bending vibration shapes of the left driving ring in the radial and tangential directions. The third order in-plane bending vibration shapes in radial and tangential directions were observed, respectively, in which the 0° position is the connection place between the sandwich composite beam and left driving ring. The measured third order bending vibration shapes in tangential and radial directions matched well with the calculation results. The measured and calculated results indicated that the two third order in-plane bending vibration shapes in tangential and radial directions have a spatial phase difference of π/2. This is the reason why the traveling wave can be generated in each driving ring at a single-phase excitation. Certainly, the maximum amplitude of the left driving ring in the radial direction is larger than that in the tangential direction, indicating that the standing wave ratio (SWR) is larger than traveling wave. Therefore, energy dissipation is inevitable as the metal track is driven by the transducer prototype. Comparisons between the experimental and simulated results adequately proved that the operating principle of the proposed transducer is feasible and the developed transfer matrix model is effective.

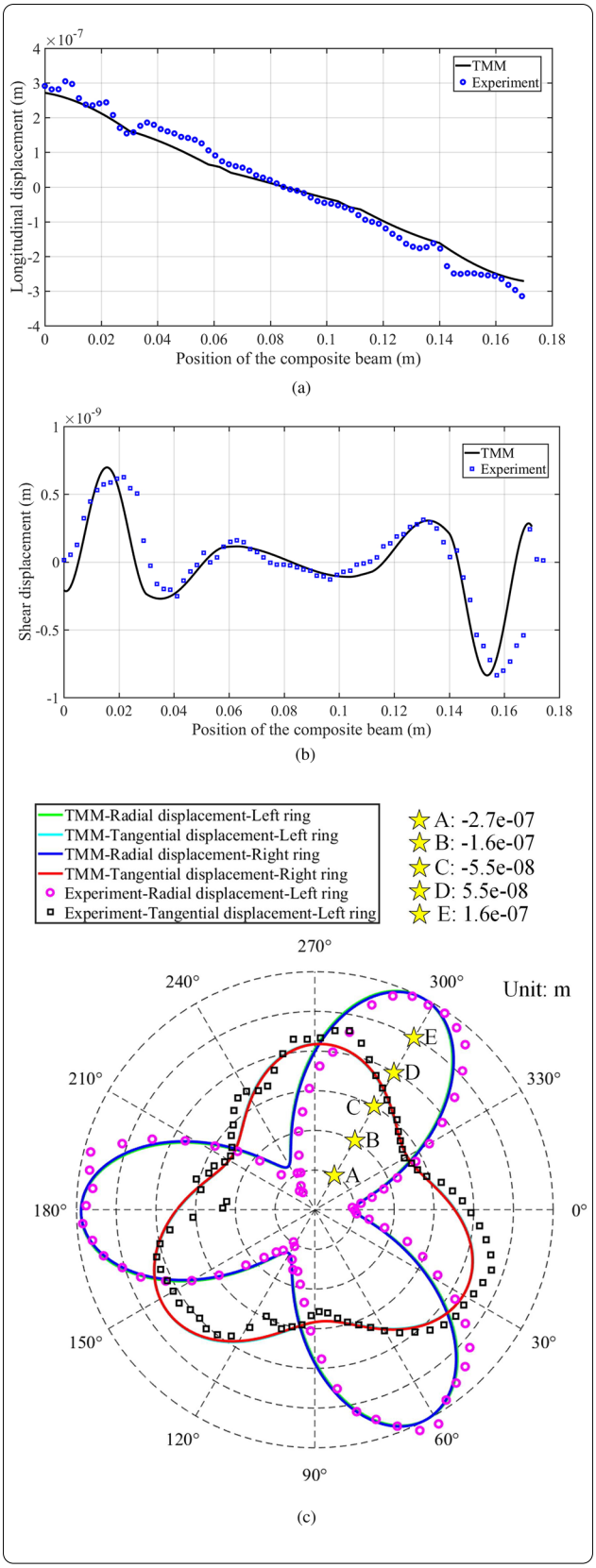

Figure 9 Vibration shapes of the transducer measured by experiments and computed by the developed analytical model: **a** Longitudinal, and **b** bending vibration shapes in the sandwich composite beam, **c** In-plane bending vibration in the left driving ring along the radial and tangential directions

5 Investigation on the Driving Concept

Since the proposed transducer is excited to produce the traveling wave in each driving ring by a single-phase signal, therefore, to investigate its driving concept is very important for further understanding of the operating principle of the transducer. Two aspects can be used to describe the driving concept clearly. One is the motion trajectory of surface points of the driving ring, and another one is the quality of the traveling wave of the driving rings. In this section, the investigations on the driving concept of the transducer are carried out.

5.1 Motion Trajectory

At first, we experimentally and theoretically investigated the motion trajectory of surface points of the driving ring. Three points (points *A*, *B*, and *C*) on the central line of the left driving ring were selected to study their motion trajectories, as shown in Figure 10(a), in which the surface region from point *A* to point *C* is used to drive the metal track and point *B* is located on the middle of this region. The excitation conditions were the same as in the last section (The corresponding frequency was 19392 Hz for the test and 19821 Hz for the calculation, and the excitation voltage is 2 V), and the motion trajectories of the selected three points are measured and plotted in Figure 10(b). Due to the fact that the central line of the left driving ring was used to analyze and describe the vibration characteristic of the transducer in our developed analytical model, the motion trajectories of the selected points were computed and compared to the experimental results, as illustrated in Figure 10(b). The measured and computed motion trajectories shown that the selected points moved elliptically, demonstrating that the proposed transducer with a single-phase excitation can achieve the effective drive on the metal track. Since the induced vibration mode is used to couple and generate traveling waves in the driving rings, the not pure traveling wave is produced in each driving ring, leading to that the standing wave ratio of each driving ring is higher than 1. This results in the trajectory difference between the points *A* and *C*.

5.2 Quality of Traveling Wave

To study the influence of geometrical dimensions on the quality of the traveling wave in the driving rings, the model-based investigation was conducted. The quality of

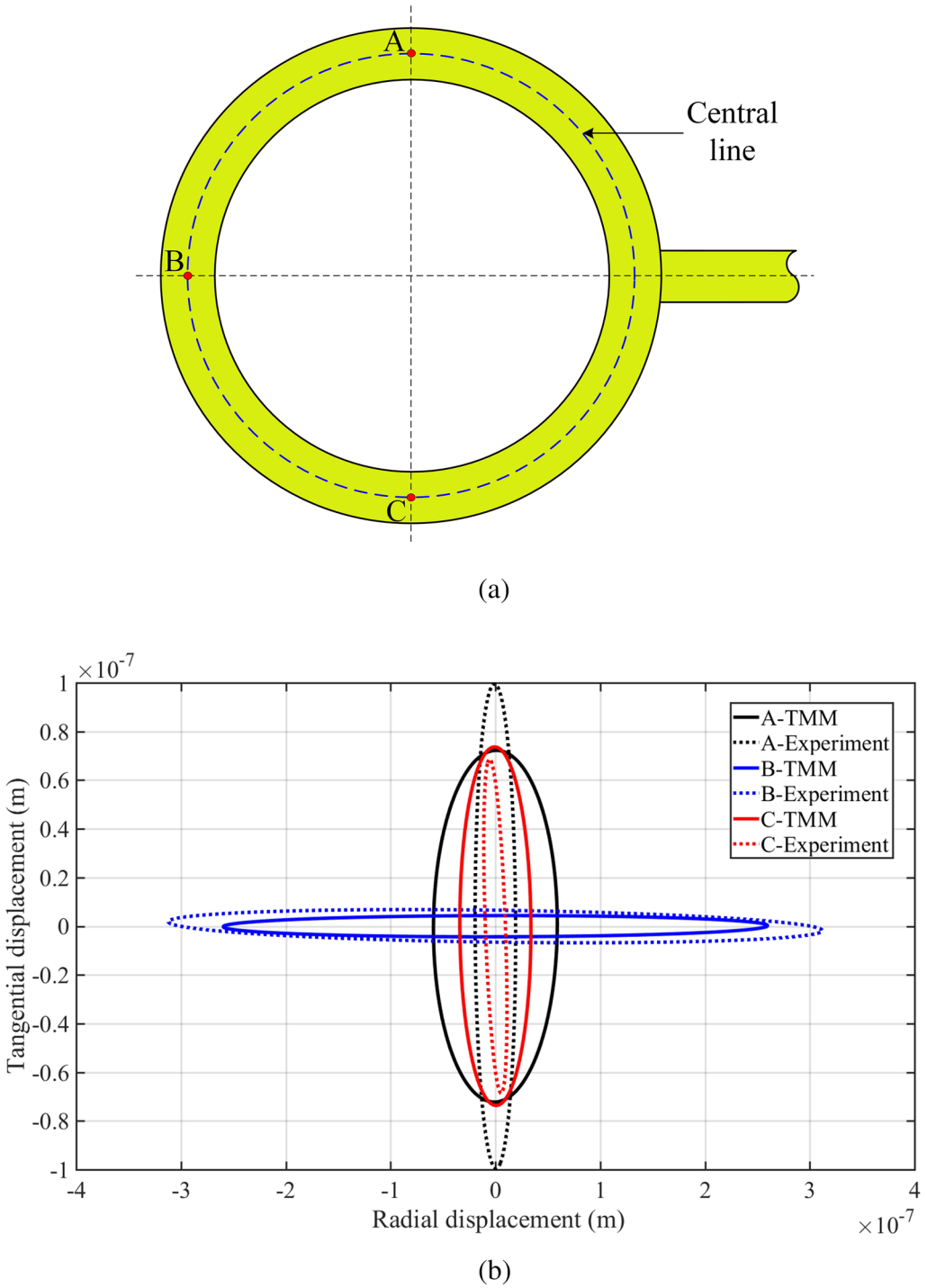

Figure 10 **a** Selected points at the central line of the left driving ring, **b** Elliptical trajectories of the selected points measured by experiments and calculated by the developed model

the traveling wave in each driving ring directly reflects the driving effect of the transducer. To quantitatively investigate the quality of the traveling wave in the driving ring, the SWR is utilized as the figure of merit. This is because the vibration of the driving ring is composed of standing wave and traveling wave at the single-phase excitation. The SWR is defined as the maximum amplitude divided by the minimum amplitude. A pure traveling

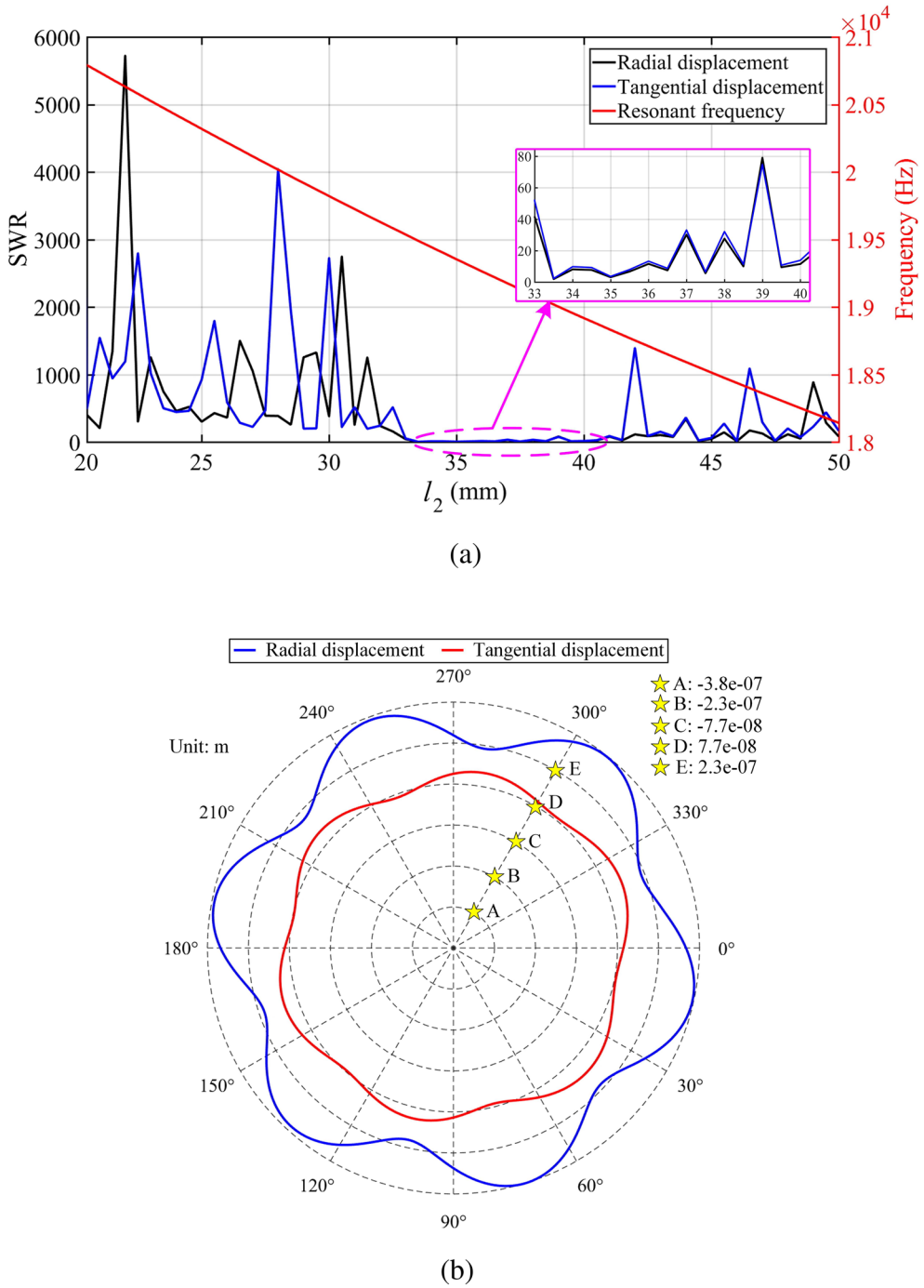

Figure 11 **a** Standing wave ratio of the left driving ring and the resonant frequency of the transducer at different length l_2, **b** Amplitudes of the left driving ring in the radial and tangential directions

wave occurs when the SWR of the driving ring is equal to 1, while a pure standing wave exists as the SWR of the driving ring is infinite. Once the SWR of the driving ring is greater than 1, it indicates that the generated traveling wave is not pure. To calculate the SWRs of the driving ring in the radial and tangential directions, the whole driving ring is first divided into 360 elements and then amplitudes of all element interfaces in both directions are computed, respectively.

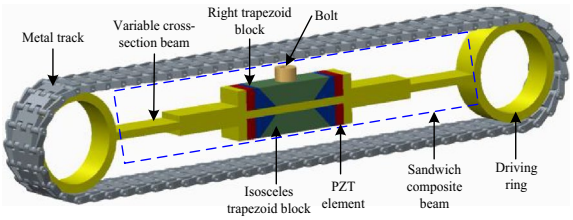

Figure 12 Configuration of the tracked mobile robot driven by the proposed traveling wave sandwich piezoelectric transducer

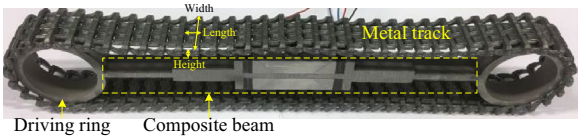

Figure 13 Prototype of the assembled tracked mobile system driven by the proposed traveling wave sandwich piezoelectric transducer

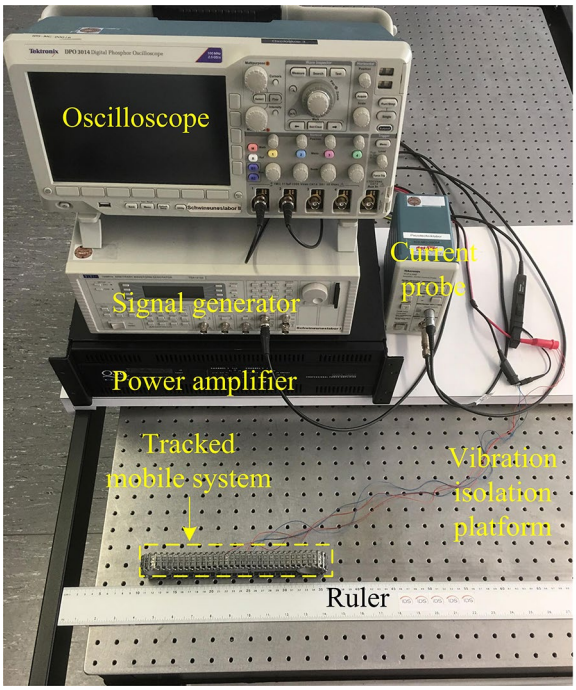

Figure 14 Experimental setup for measuring the motion characteristics of the assembled tracked mobile system prototype

Due to the fact that the tangential displacement of surface points of the driving ring is induced by the structural coupling between the sandwich composite beam and driving ring, it means that the generated traveling wave would be disturbed by standing wave. To investigate the influence of geometrical dimensions on the SWR of the driving ring, we conducted calculations. At first, we studied the influence of the inner radius (R_1) and outer radius (R_2) of the driving ring individually. When R_1 was varied from 15 mm to 16 mm in steps of 0.1 mm or R_2 was changed from 19 mm to 20 mm in steps of 0.1 mm, the minimum SWR of the left driving ring is more than 100 in both directions, indicating that these two geometrical dimensions have a small influence on the SWR. Then we investigated the influence of the length (l_2) of the elastic beam element connecting with the driving ring. The computed SWRs of the left driving ring in the radial and tangential directions are plotted in Figure 11(a), when l_2 varied from 20 mm to 50 mm with a step of 0.5 mm. It can be observed that a specific length range existed as l_2 varied from 33 mm to 40 mm, due to the fact that the SWRs of the left driving ring in both directions at this length range are relatively smaller than other lengths. The minimum SWRs for the radial and tangential directions are 2.282 and 1.914, respectively, both corresponding to the value of l_2 of 33.5 mm, meaning that the quality of the traveling wave in the driving ring is highest at this length. It also can be seen that the resonant frequency of the operating vibration mode of the transducer linearly decreased with the increase of l_2. Selected the length of l_2 of 33.5 mm and its corresponding resonant frequency of 19490 Hz as the driving frequency, the amplitudes of the left driving ring in both directions are computed and plotted in Figure 11(b). It can be found that the amplitude of the driving ring in the radial direction is larger than that in the tangential direction. This indicates that the output force of the metal track driven by the transducer is better than its output velocity. In a word, the length of l_2 can be used as the key geometrical dimension to improve the quality of the traveling wave in the driving rings under a single-phase excitation.

6 Application Example Investigation

To verify the driving effect of the proposed traveling wave sandwich piezoelectric transducer, an application example is presented in this section. In Refs. [29, 30], tracked mobile systems driven by traveling wave piezoelectric transducers with two phases excitation signals have been investigated. A metal track is adopted as the rotor to be driven by a piezoelectric transducer via friction. Compared to traditional driving forms utilizing electromagnetic motors and retarding mechanisms, the piezoelectric actuated method greatly simplifies the configuration of the tracked mechanism, eliminating the problem of lubricant volatilization and deflation within

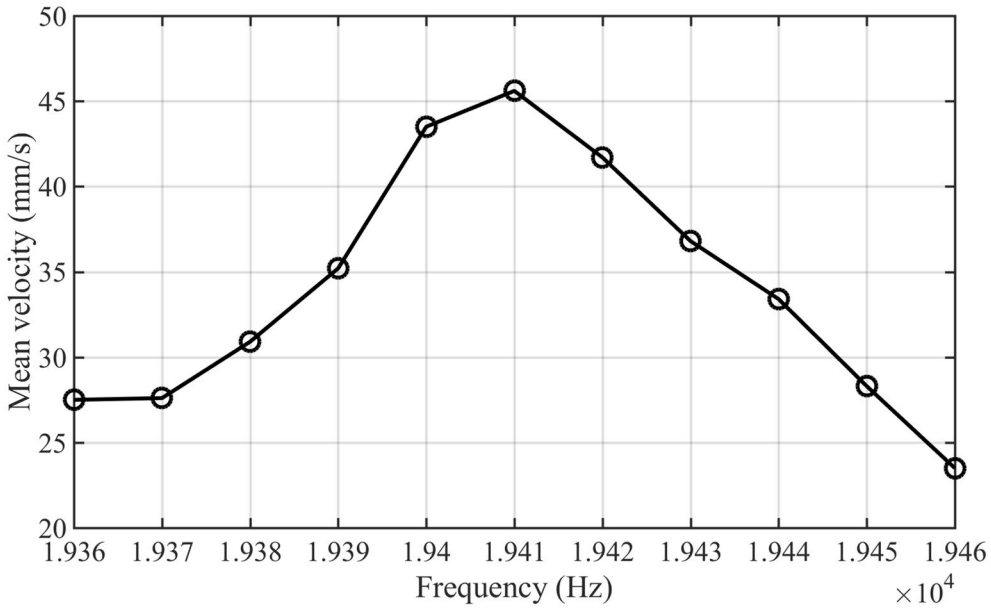

Figure 15 Frequency sensitivity measurement results

operating in vacuum environments, and is free from electromagnetic interference. Therefore, the approach utilizing piezoelectric transducers to drive track presents potential application for planetary explorations. Referring to our previous designs, the application example of this proposed transducer is still to build a tracked mobile system, as shown in Figure 12. A metal track with smooth inner surface is tensioned along the outer surfaces of the two driving rings of the proposed traveling wave sandwich piezoelectric transducer.

The prototype of the tracked mobile system with the weight of 395 g was assembled, as shown in Figure 13. The dimensions of each track block are 2.76 mm in height, 13 mm in width, and 7.52 mm in length. In this section, we conducted experimental investigations on the tracked mobile system prototype to verify the driving performance of the transducer. To measure motion characteristics of the tracked mobile system, an experimental setup was built, as shown in Figure 14. It includes a power amplifier, a signal generator, an oscilloscope, and a current probe. The prototype of the tracked mobile system with a single-phase excitation moved on a vibration isolation platform, and its motion situations were recorded by a camera. Thus, the motion characteristics of the assembled tracked mobile system were obtained by evaluating the videos.

6.1 Frequency Sensitivity Measurement

Although the resonant frequency of the operating principle of the transducer prototype has been determined, the assembly of the metal track changes its boundary conditions. Therefore, we conducted the frequency sensitivity measurement to find an optimal driving frequency with the maximum mean velocity for the tracked mobile system prototype. The experimental results are plotted in Figure 15. The excitation voltage applied to the system prototype was 300 V_{RMS}. The driving frequency varied from 19360 Hz to 19460 Hz with a step of 10 Hz. The results showed that the mean velocity of the system prototype first increased and then decreased when the driving frequency increased, leaving an optimal driving frequency of 19410 Hz corresponding to the maximum mean velocity of the system prototype of 45.6 mm/s. Compared to the measured resonant frequency of the transducer prototype in the last section, the obtained driving frequency of the assembled system was shifted by 18 Hz. This indicates that the installation of the metal track changed the resonant frequency of the transducer prototype, due to the fact that its vibration property was primarily influenced by the contact stiffness between the transducer and the metal track.

6.2 Motion Characteristic

Based on the measured optimal driving frequency of 19410 Hz, motion characteristics of the system prototype were tested under different voltages by using the aforementioned experimental setup (Figure 14), as illustrated in Figure 16. The motion characteristic curve showed that the mean velocity of the system prototype rose with the increase of the excitation voltage. It can be found that

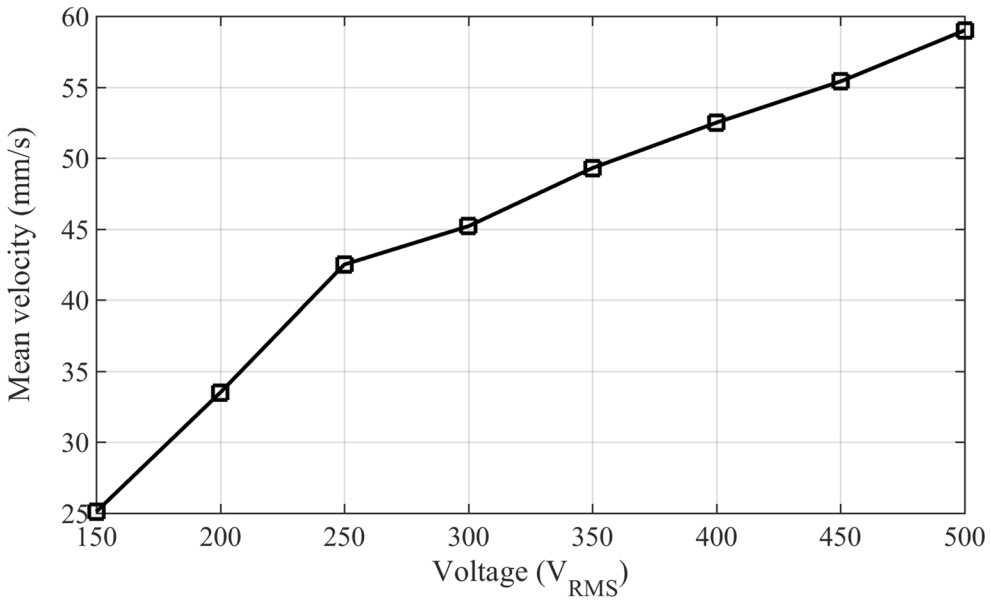

Figure 16 Motion characteristic of the system prototype under different excitation voltages

a specific mean velocity of the system prototype occurred in the excitation voltage of 250 V_{RMS}, making that the motion characteristic curve varied non-linear. This is caused by the accumulation of experimental errors due to the fact that each measured mean velocity was calculated in terms of the experimental results of 5 times. The maximum mean velocity of 59 mm/s was obtained when the excitation voltage was 500 V_{RMS}. The results demonstrated that the transducer prototype can drive the metal track while it was excited with a single-phase voltage varied from 150 V_{RMS} to 500 V_{RMS}.

6.3 Traction Performance

The traction force is generally adopted as an important index for evaluating the performance of the mobile system. For our assembled tracked mobile system, we built an experimental setup to test its traction performance, as illustrated in Figure 17(a). To avoid slide phenomenon during measurements of the assembled system, the surface of the vibration isolation platform was covered with abrasive papers with the roughness of P100 (Germany standard). The measured optimal frequency of 19410 Hz was still used as the driving frequency for traction performance measurements of the prototype.

First, the maximum stalling traction performance was measured under different excitation voltages, and the results were plotted in Figure 17(b). The maximum stalling traction force increased linearly when the excitation voltage increased. When the voltage was 500 V_{RMS}, the maximum stalling traction force reached up to 1.65 N. For real applications, the traction performance of the tracked mobile system should be improved.

Additionally, the loading characteristic of the system prototype was measured using the same experimental setup when the excitation voltage was 300 V_{RMS}, as shown in Figure 17(c). With the loading weight increased, the mean velocity of the system prototype decreased. At each loading weight, the mean velocity of the system prototype was calculated according to the experimental results of 5 times. These results preliminarily present the noteworthy driving performances of the proposed traveling wave sandwich piezoelectric transducer with a single-phase excitation.

6.4 Comparisons

The measured performances of the single phase excited tracked mobile system are compared to some developed traveling wave tracked mobile systems under the two excitation voltages, as listed in Table 3. The maximum mean velocity and loading weight of the tracked mobile system driven by a surface-bonded type piezoelectric

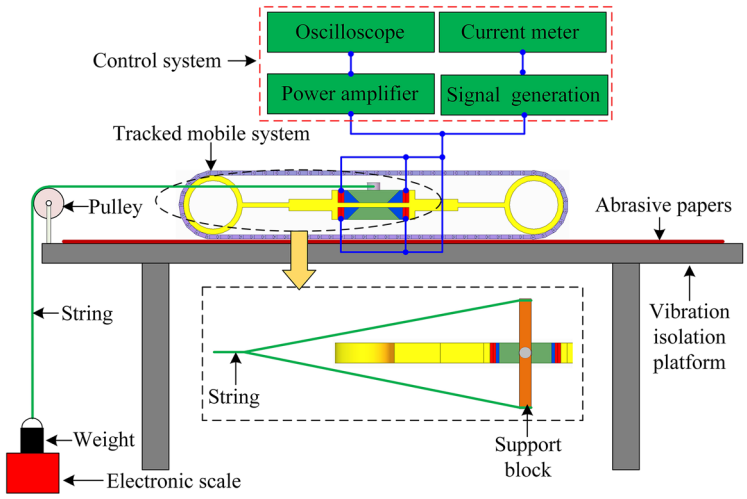

(a)

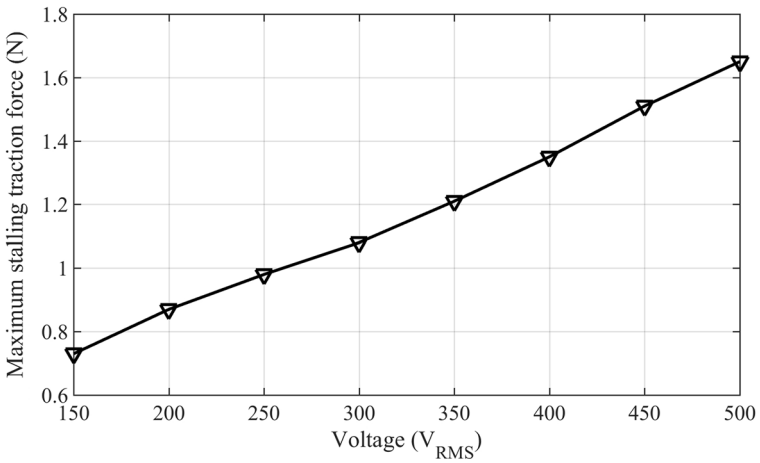

(b)

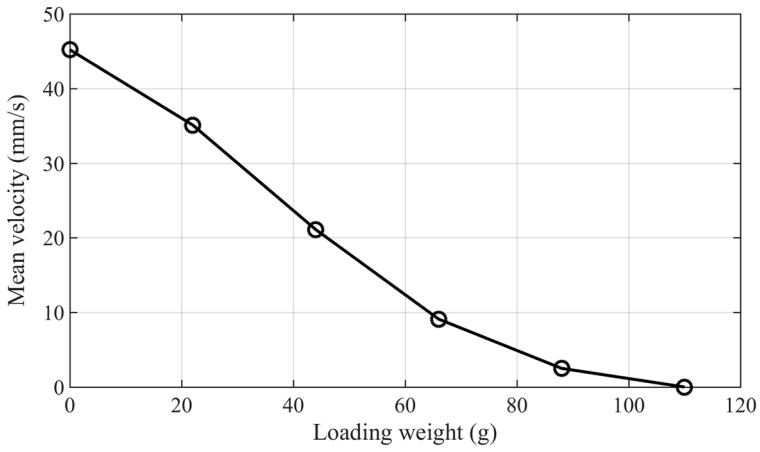

(c)

Figure 17 **a** Experimental setup for measuring traction performance of the system prototype, **b** Maximum stalling traction force measured under different excitation voltages, **c** The relationship between the mean velocity and the loading weight under the excitation voltage of 300 V_{RMS}

Table 3 Comparisons between the proposed tracked mobile system and some developed traveling wave tracked mobile systems

Parameters	Tracked mobile system driven by a surface-bonded type piezoelectric transducer with four driving rings [29]	Tracked mobile system driven by a sandwich piezoelectric transducer with two driving rings [30]	The proposed tracked mobile system
Driving frequency (kHz)	65.31	35.1	19.41
Weight(g)	244	403	395
Dimensions of the piezoelectric transducer (mm × mm × mm)	164.9 × 44.6 × 8	198 × 40 × 12	247 × 38.5 × 12
Maximum mean velocity	57 mm/s under two excitation voltages of 460 V_{RMS}	72 mm/s under two excitation voltages of 500 V_{RMS}	59 mm/s under the excitation voltage of 500 V_{RMS}
Maximum stalling force (N)	Not available	Not available	1.65
Maximum loading weight	240 g under two excitation voltages of 400 V_{RMS}	1.44 kg under two excitation voltages of 300 V_{RMS}	110 g (traction loading weight) under the excitation voltage of 300 V_{RMS}

transducer with four driving rings [29] are 57 mm/s and 240 g under two excitation voltages of 460 V_{RMS}, respectively. The tracked mobile system driven by a sandwich piezoelectric transducer with two driving rings [30] achieved a maximum mean velocity of 72 mm/s under two excitation voltages of 500 V_{RMS} and a maximum loading weight of 1440 g under two excitation voltages of 300 V_{RMS}. Although the maximum mean velocity of the proposed tracked mobile system is a little lower than the aforementioned two tracked mobile systems, it only required a single-phase excitation voltage, simplifying the control system. It should be pointed out that the loading weight for the tracked mobile system in Refs. [29, 30] indicates the actual loading while our measured loading weight in the last section represents the traction force for the assembled system prototype, thus, the comparison is not given for these three tracked mobile systems.

7 Conclusions

(1) A novel traveling wave sandwich piezoelectric transducer with single phase excitation was proposed, theoretically analyzed, experimentally validated and investigated in this study. Using the structural coupling property between the sandwich composite beam and driving rings, the proposed piezoelectric transducer can produce traveling waves in the driving rings under a single-phase excitation signal, greatly simplifying the control system.

(2) An overall transfer matrix model was first created to describe the dynamic behavior of the proposed traveling wave sandwich piezoelectric transducer.

(3) Then the vibration measurements were carried out on the transducer prototype and compared to the calculation results. The comparisons showed that the computed vibration characteristics of the transducer were in good agreement with the measured results, demonstrating the effectiveness of the developed transfer matrix model and confirming the operating principle of the proposed transducer.

(4) Additionally, the elliptical trajectories of the surface points of the driving ring were obtained, and the influence of geometrical dimensions on the quality of traveling wave of the driving ring was investigated, showing that the computed minimum SWRs of the driving ring in the radial and tangential directions are 2.282 and 1.914, respectively, at the value of l_2 of 33.5 mm.

(5) Finally, a case study on evaluating the driving performance of the proposed traveling wave sandwich piezoelectric transducer was carried out by constructing and assembling a tracked mobile system. The frequency sensitivity results indicated that the driving frequency of the system prototype was 19410 Hz corresponding to the maximum mean velocity and shifting 18 Hz compared to the measured resonant frequency of the transducer prototype. The maximum mean velocity and maximum stalling traction force of the system prototype were respectively 59 mm/s and 1.65 N when the excitation voltage was 500 V_{RMS}. The mean velocity of the system prototype decreased when the loading weight increased. These experimental results demonstrated that the driving effect of the proposed

traveling wave sandwich piezoelectric transducer with a single-phase excitation deserves attention.

Appendices

Appendix A

The components of the longitudinal vibration transfer matrix $\boldsymbol{T_{sL}}$ of the sandwich beam are expressed as follows:

$$T_{sL,11}=\frac{T_{pL,12}T_{iL,11}+2T_{iL,12}T_{pL,11}}{2T_{iL,12}+T_{pL,12}},\quad T_{sL,12}=\frac{T_{iL,12}T_{pL,12}}{2T_{iL,12}+T_{pL,12}},$$
$$T_{sL,13}=\frac{2T_{iL,12}T_{pL,13}}{2T_{iL,12}+T_{pL,12}},$$
$$T_{sL,21}=2T_{pL,21}+T_{iL,21}+\frac{2(T_{pL,22}-T_{iL,22})(T_{iL,11}-T_{pL,11})}{2T_{iL,12}+T_{pL,12}},$$
$$T_{sL,22}=\frac{T_{pL,12}T_{iL,22}+2T_{iL,12}T_{pL,22}}{2T_{iL,12}+T_{pL,12}},$$
$$T_{sL,23}=2T_{pL,23}+\frac{2T_{pL,13}(T_{iL,22}-T_{pL,22})}{2T_{iL,12}+T_{pL,12}},$$
$$T_{sL,31}=2T_{pL,31}+2T_{pL,32}\frac{T_{iL,11}-T_{pL,11}}{2T_{iL,12}+T_{pL,12}},$$
$$T_{sL,32}=\frac{2T_{iL,12}T_{pL,32}}{2T_{iL,12}+T_{pL,12}},\text{ and }T_{sL,33}=2T_{pL,33}-\frac{2T_{pL,13}T_{pL,32}}{2T_{iL,12}+T_{pL,12}}.$$

Appendix B

The components of the bending vibration transfer matrix $\boldsymbol{T_{iB}}$ of the elastic beam i are given as follows:

$$T_{iB,11}=c_{0i}-\sigma_i c_{2i},\quad T_{iB,12}=-l_i[c_{1i}-(\sigma_i+\tau_i)c_{3i}],$$
$$T_{iB,13}=-j\omega a_i c_{2i},\quad T_{iB,14}=\frac{-j\omega a_i l_i\left[(\beta_i^4+\sigma_i^2)c_{3i}-\sigma_i c_{1i}\right]}{\beta_i^4},$$
$$T_{iB,21}=-\frac{\beta_i^4 c_{3i}}{l_i},\ T_{iB,22}=c_{0i}-\tau_i c_{2i},\ T_{iB,23}=\frac{j\omega a_i(c_{1i}-\tau_i c_{3i})}{l_i},$$
$$T_{iB,24}=-T_{ib,13},\quad T_{iB,31}=-\frac{\beta_i^4 c_{2i}}{j\omega a_i},$$
$$T_{iB,32}=\frac{l_i\left[(\beta_i^4+\tau_i^2)c_{3i}-\tau_i c_{1i}\right]}{j\omega a_i},\quad T_{iB,33}=T_{iB,22},$$
$$T_{iB,34}=-T_{iB,12},\ T_{iB,41}=-\frac{\beta_i^4(c_{1i}-\sigma_i c_{3i})}{j\omega a_i l_i},\ T_{iB,42}=-T_{iB,31},$$
$$T_{iB,43}=-T_{iB,21},\quad\text{and}\quad T_{iB,44}=T_{iB,11},\quad\text{in which}$$

$$\begin{cases} c_{0i}=\dfrac{\lambda_{2i}^2\cosh\lambda_{1i}+\lambda_{1i}^2\cos\lambda_{2i}}{\lambda_{1i}^2+\lambda_{2i}^2} \\ c_{1i}=\dfrac{\frac{\lambda_{2i}^2}{\lambda_{1i}}\sinh\lambda_{1i}+\frac{\lambda_{1i}^2}{\lambda_{2i}}\sin\lambda_{2i}}{\lambda_{i1}^2+\lambda_{i2}^2} \\ c_{2i}=\dfrac{\cosh\lambda_{1i}-\cos\lambda_{2i}}{\lambda_{1i}^2+\lambda_{2i}^2} \\ c_{3i}=\dfrac{\frac{1}{\lambda_{1i}}\sinh\lambda_{1i}-\frac{1}{\lambda_{2i}}\sin\lambda_{2i}}{\lambda_{1i}^2+\lambda_{2i}^2} \\ \lambda_{1i,2i}=\sqrt{\sqrt{\beta_i^4+\frac{(\sigma_i-\tau_i)^2}{4}}\mp\frac{\sigma_i+\tau_i}{2}} \end{cases}\quad\text{with}\quad \sigma_i=\frac{\mu_i\omega^2}{(GA)_i}l_i^2,$$

$\tau_i=\frac{(\rho I)_i\omega^2}{(EI)_i}l_i^2$, $\beta_i^4=\frac{\mu_i\omega^2}{(EI)_i}l_i^4$, and $a_i=\frac{l_i^2}{(EI)_i}$, where $(GA)_i=\kappa^2 Wh_iG_i$ is the shear stiffness, $(EI)_i=Wh_i^3E_i/12$ is the bending stiffness, $(\rho I)_i=Wh_i^3\rho_i/12$ is the moment of inertia, $\mu_i=Wh_i\rho_i$ is the mass, G_i is the shear modulus, and κ is the correction factor depending on the elastic beam cross-section.

Acknowledgements
Not applicable.

Authors' contributions
LW proposed the novel design of the piezoelectric transducer and developed its dynamical analytical model. FB guided in analyzing the operating principle of the piezoelectric transducer. VH conducted the dynamical analytical modeling of the piezoelectric transducer and experimental verification. LW and JJ carried out the experimental investigation on the case study of assembled tracked mobile system. LW and JT were in charge of the whole structure of the manuscript. All authors contributed to the preparation of the manuscript. All authors read and approved the final manuscript.

Authors' Informations
Liang Wang is currently a lecturer in Mechanical Engineering at *Nanjing University of Aeronautics and Astronautics, China*. He received his doctoral degree from *Nanjing University of Aeronautics and Astronautics, China,* in 2018. His research interest includes piezoelectric actuators, mobile robotic systems, and ultrasonic motors.
Fushi Bai is currently an associate professor in Marine Science and Technology at *Northwestern Polytechnical University, China*. He received his doctoral degree in mechanical engineering from *Leibniz University Hannover, Germany,* in 2019. He mainly focuses on ultrasonic cavitation and peening process.
Viktor Hofmann received the Diploma degree in mechanical engineering from *Leibniz University Hannover, Germany*, in 2013. He is currently working toward the Ph.D. degree in the *Institute of Dynamics and Vibration Research, Leibniz University Hannover, Germany*, researching in piezoelectric actuators, and tactile display.
Jiamei Jin is currently a Professor with *the State Key Laboratory of Mechanics and Control of Mechanical Structures* at *Nanjing University of Aeronautics and Astronautics, China.* He received the Ph.D. degree in mechatronics engineering from *Nanjing University of Aeronautics and Astronautics, China,* in 2007. His research interests include piezoelectric actuators, ultrasonic motors, ultrasonic machining, and robotics.
Jens Twiefel received the Diploma degree in mechanical engineering from *University of Paderborn*, *Germany*, in 2004, and the Ph.D. degree in mechanical engineering from *the Institute of Dynamics and Vibration Research, Leibniz University Hannover*, *Germany*, in 2010. From 2004 to 2007, he was a research assistant at Mechatronics and Dynamics of *Heinz Nixdorf Institute, University of Paderborn*. Since 2007, he is a research assistant in the *Institute of Dynamics and Vibration Research, Leibniz University Hannover*, *Germany,* in which, he is promoted as the head of Piezoelectric and Ultrasonic Technology Research Group in the *Institute of Dynamics and Vibration Research* since 2008. His research interests include piezoelectric transducers, ultrasonic motors, ultrasonic machining, and vibration energy harvesting.

Funding
Supported by the National Science Foundation of China (Grants Nos. 51905262 and U2037603), the Natural Science Foundation of Jiangsu Province (Grant No. BK20190398), and the State Key Laboratory of Mechanical System and Vibration (Grant No. MSV202011).

Competing Interests
The authors declare no competing financial interests.

Author Details
[1]State Key Laboratory of Mechanics and Control of Mechanical Structures, Nanjing University of Aeronautics and Astronautics, Nanjing 210016, China. [2]Institute of Dynamics and Vibration Research, Leibniz University Hannover, 30167 Hannover, Germany. [3]School of Marine Science and Technology, Northwestern Polytechnical University, Xi'an 710072, Shaanxi, China.

Received: 3 August 2020 Revised: 1 September 2021 Accepted: 12 October 2021
Published online: 03 November 2021

References

[1] K Uchino. *Advanced piezoelectric materials: Science and technology*. Springer, 2017.
[2] D Mazeika, P Vasiljev. Linear inertial piezoelectric motor with bimorph disc. *Mechanical Systems and Signal Processing*, 2013, 36: 110–117.
[3] J Wu, Y Mizuno, K Nakamura. Polymer-based ultrasonic motors utilizing high-order vibration modes. *IEEE/ASME Transactions on Mechatronics*, 2018, 23: 788–799.
[4] Y Liu, J Yan, D Xu, et al. An I-shape linear piezoelectric actuator using resonant type longitudinal vibration transducers. *Mechatronics*, 2016, 40: 87–95.

[5] D Yamaguchi, T Kanda, K Suzumori. An ultrasonic motor for cryogenic temperature using bolt-clamped Langevin-type transducer. *Sensors and Actuators A: Physical*, 2012, 184: 134–140.
[6] A Mustafa, T Morita. Dynamic preload control of traveling wave rotary ultrasonic motors for energy efficient operation. *Japanese Journal of Applied Physics*, 2019, 58: SGGD04.
[7] T Mashimo. Scaling of piezoelectric ultrasonic motors at submillimeter range. *IEEE/ASME Transactions on Mechatronics*, 2017, 22: 1238–1246.
[8] X Li, D Chen, J Jin, et al. A novel underwater piezoelectric thruster with one single resonance mode. *Review of Scientific Instruments*, 2019, 90: 045007.
[9] M Kurosawa, S Ueha. Single-phase drive of a circular ultrasonic motor. *Journal of the Acoustical Society of America*, 1991, 90: 1723–1728.
[10] O Vyshnevskyy, S Kovalev, W Wischnewskiy. A novel, single-mode piezoceramic plate actuator for ultrasonic linear motors. *IEEE Transactions on Ultrasonics, Ferroelectrics, and Frequency Control*, 2005, 52: 2047–2053.
[11] H Tamura, K Shibata, M Aoyagi, et al. Single phase drive ultrasonic motor using $LiNbO_3$ rectangular vibrator. *Japanese Journal of Applied Physics*, 2008, 47: 4015–4020.
[12] S He, P Chiarot, S Park. A single vibration mode tubular piezoelectric ultrasonic motor. *IEEE Transactions on Ultrasonics, Ferroelectrics, and Frequency Control*, 2011, 58: 1049–1061.
[13] K Yokoyama, H Tamura, K Masuda, et al. Single-phase drive ultrasonic linear motor using a linked twin square plate vibrator. *Japanese Journal of Applied Physics*, 2013, 52: 07HE03.
[14] Z Liu, Z Yao, X Li, et al. Design and experiments of a linear piezoelectric motor driven by a single mode. *Smart Materials and Structures*, 2016, 87: 115001.
[15] L K Chang, M C Tsai. Design of single-phase driven screw-thread-type ultrasonic motor. *Review of Scientific Instruments*, 2016, 87: 055002.
[16] Y Ma, M Choi, K Uchino. Single-phase driven ultrasonic motor using two orthogonal bending modes of sandwiching piezo-ceramic plates. *Review of Scientific Instruments*, 2016, 87: 115004.
[17] V Dabbagh, A Sarhan, J Akbari, et al. Design and experimental evaluation of a precise and compact tubular ultrasonic motor driven by a single-phase source. *Precision Engineering*, 2017, 48: 172–180.
[18] P Fan, X Shu, T Yuan, et al. A novel high thrust–weight ratio linear ultrasonic motor driven by single-phase signal. *Review of Scientific Instruments*, 2018, 89: 085001.
[19] B Zhang, Z Yao, Z Liu, et al. A novel L-shaped linear ultrasonic motor operating in a single resonance mode. *Review of Scientific Instruments*, 2018, 89: 015006.
[20] E Pestel, F Leckie. *Matrix methods in elastomechanics*. MGgrow-Hill, 1963.
[21] V Hofmann, J Twiefel. Optimization of a piezoelectric bending actuator for a tactile display. *Energy Harvesting and Systems*, 2015, 2: 177–185.
[22] V Hofmann, J Twiefel. Self-Sensing with loaded piezoelectric bending actuators. *Sensors and Actuators A: Physical*, 2017, 263: 737–743.
[23] L Wang, T Wielert, J Twiefel, et al. A rod type linear ultrasonic motor utilizing longitudinal traveling waves: proof of concept. *Smart Materials and Structures*, 2017, 26: 085013.
[24] L Wang, V Hofmann, F Bai, et al. Systematic electromechanical transfer matrix model of a novel sandwiched type flexural piezoelectric transducer. *International Journal of Mechanical Sciences*, 2018, 138–139: 229–2433.
[25] L Wang, V Hofmann, F Bai, et al. Modeling of coupled longitudinal and bending vibrations in a sandwich type piezoelectric transducer utilizing the transfer matrix method. *Mechanical Systems and Signal Processing*, 2018, 108: 216–237.
[26] L Wang, V Hofmann, F Bai, et al. A novel additive manufactured three-dimensional piezoelectric transducer: Systematic modeling and experimental validation. *Mechanical Systems and Signal Processing*, 2019, 114: 346–365.
[27] T Irie, G Yamada, K Tanaka. Nature frequencies of in-plane vibration of arcs. *Journal of Applied Mechanics*, 1983, 50: 449–452.
[28] V Hofmann, G Kleyman, J Twiefel. Modeling and experimental investigation of a periodically excited hybrid energy-harvesting generator. *Energy Harvesting and Systems*, 2015(2): 213–226.
[29] L Wang, C Shu, J Jin, et al. A novel traveling wave piezoelectric actuated tracked mobile robot utilizing friction effect. *Smart Materials and Structures*, 2017, 26: 035003.
[30] L Wang, C Shu, Q Zhang, et al. A novel sandwich-type traveling wave piezoelectric tracked mobile system. *Ultrasonics*, 2017, 75: 28–35.